

Correlation and localization properties of topological charge density and the pseudoscalar glueball mass in SU(3) lattice Yang-Mills theory

Abhishek Chowdhury,¹ A. Harindranath,¹ and Jyotirmoy Maiti²

¹*Theory Division, Saha Institute of Nuclear Physics
1/AF Bidhan Nagar, Kolkata 700064, India*

²*Department of Physics, Barasat Government College,
10 KNC Road, Barasat, Kolkata 700124, India**

(Dated: March 11, 2015)

Towards the goal of extracting the continuum properties, we have studied the Topological Charge Density Correlator (TCDC) and the Inverse Participation Ratio (IPR) for the topological charge density ($q(x)$) in SU(3) Lattice Yang-Mills theory for relatively small lattice spacings including some smaller than those explored before. With the help of recently proposed open boundary condition, it is possible to compute observables at a smaller lattice spacing since *trapping problem* is absent. On the other hand, the reference energy scale provided by Wilson flow allows us to study their scaling behavior in contrast to previously proposed smearing techniques. The behavior of TCDC for different lattice spacings at a fixed HYP smearing level shows apparent scaling violations. In contrast, at a particular Wilson flow time t for all the lattice spacings investigated (except the largest one), the TCDC data show universal behavior within our statistical uncertainties. The continuum properties of TCDC are studied by investigating the small flow time behavior. We have also extracted the pseudoscalar glueball mass from TCDC, which appears to be insensitive to the lattice spacings ($0.0345 \text{ fm} \leq a \leq 0.0667 \text{ fm}$) and agrees with the value extracted using anisotropic lattices, within statistical errors. Further, we have studied the localization property of $q(x)$ through IPR whose continuum behavior can be probed through the small values of Wilson flow time and observed the decrease of IPR with decreasing Wilson flow time. A detailed study of $q(x)$ under Wilson flow time revealed that as Wilson flow time decreases, the proximity of the regions of positive and negative charge densities of large magnitudes increases, and the charge density appears to be more delocalized resulting in the observed behavior of IPR.

PACS numbers: 11.15.-q, 11.15.Ha, 12.38.-t, 12.38.Gc, 12.39.Mk

* abhishek.chowdhury@saha.ac.in; a.harindranath@saha.ac.in; jyotirmoy.maiti@gmail.com

I. INTRODUCTION AND MOTIVATION

The negativity of the Topological Charge Density Correlator (TCDC) for non-zero distances as a consequence of the reflection positivity and the pseudoscalar nature of the relevant local operator in Euclidean field theory is well-known [1, 2]. The non-trivial implication of the negativity of TCDC for the structure of topological charge density in QCD vacuum has been investigated in detail [3]. Various aspects of TCDC in quenched and full QCD have been carried out in Refs. [4–13]. The four volume integral of TCDC gives the topological susceptibility χ . A thorough investigation of the mechanisms leading to the suppression of the topological susceptibility with decreasing quark mass, based on the properties of TCDC has been carried out [11] in two-flavour QCD. The famous Witten-Veneziano formula [14, 15] relates η' mass to the topological susceptibility in pure Yang-Mills theory.

For the calculation of the topological charge density $q(x)$, various definitions have been used in the literature. Ref. [16] uses the algebraic definition of the field strength tensor. To overcome the potential lattice artifacts associated with the algebraic definition of the topological charge density $q(x)$ on the lattice and severe singularities present in TCDC in the continuum theory, various proposals have been studied in the literature. In Ref. [17], $q(x)$ based on Ginsparg-Wilson fermion has been employed, whereas Refs. [18, 19] utilize a proposal designed to overcome short distance singularities. A spectral projection formula designed to be free from singularity is employed in Ref. [20] which compares the result for topological susceptibility χ using algebraic definition. Since Ref. [20] has established that the results for χ using various approaches are in agreement with each other within statistical uncertainties, in this work we employ the algebraic (clover) definition for $q(x)$ unless otherwise stated.

There remain several open issues related to the topological charge density $q(x)$ and TCDC in non-abelian gauge theories. An important issue is the scaling of TCDC as one approaches the continuum limit. It is however well-known that current lattice gauge theory simulations employing periodic boundary condition in the temporal direction are handicapped by the trapping of topological charge in a particular sector, as the lattice spacing is reduced so as to reach the continuum limit. Open boundary condition in the temporal direction has been proposed and investigated [21–23] as a (partial) cure to this problem. Open boundary condition also has been advantageously used in the investigation of SU(2) lattice gauge theory at weak coupling in Ref. [24]. With open boundary condition, one can probe TCDC for even smaller lattice spacings and address questions related to the scaling etc.

With the adoption of the algebraic definition of $q(x)$, to suppress unwanted lattice artifacts, smearing of gauge fields is necessary. In our past study of TCDC [11], we have employed HYP smearing [25]. However, the recently proposed Wilson flow [26–28] makes smearing a well-defined mathematical procedure and in addition, provides a common reference scale to extract physical quantities from lattice calculations employing different lattice spacings. The continuum properties of observables such as TCDC can be studied by investigating the small flow time behavior. The scale provided by Wilson flow has been used in pure Yang-Mills theory to compare topological susceptibility calculated at different lattice spacings [29]. Similar scaling study for topological susceptibility has been performed recently also for dynamical fermions [12].

With the help of open boundary condition, we have been able to extract [30] scalar glueball mass down to a lattice spacing of 0.0345 fm which was not accessible with periodic boundary condition. It will be also very interesting to extract the pseudoscalar glueball mass with the same ensembles of configurations, from the tail region of the TCDC.

In addition to the properties of the correlator of topological charge density, its localization property itself is also of interest. There exists a body of literature on the localization properties of the low-lying Dirac eigen modes [31], because of their connection with the topological properties of the QCD vacuum. However, the localization properties of the topological charge density based on the algebraic definition involving the field strength $F_{\mu\nu}$ seems to have attracted little attention except for a preliminary study by the MILC collaboration [32]. It is interesting to study the Inverse Participation Ratio (IPR) associated with the topological charge density distribution and compare their behavior under Wilson flow and HYP smearing. A direct visualization of the effect of Wilson flow on topological charge density distribution of typical gauge configurations will also shed light on their localization properties.

II. SIMULATION PARAMETERS

In table I, we present simulation parameters for the HMC algorithm used to generate configurations with open and periodic boundary condition in the temporal direction with unimproved $SU(3)$ Wilson gauge action. We also give the number of configurations used for measurements of TCDC and IPR. The ‘Gap’ multiplied by τ denotes the trajectory interval between two successive measurements. We have chosen the gaps from our studies of autocorrelation for TCDC at a fixed value of r (in units of fm), such that the measurements are statistically independent of each other. The ensemble P_3 is an exception, as because of significantly smaller ensemble size in this case (due to larger value of β and periodic boundary), it was not possible to maintain large enough gaps between successive measurements. Hence,

Lattice	Volume	β	N_{cnfg}	Gap	τ	$a[\text{fm}]$	t_0/a^2
O_1	$24^3 \times 48$	6.21	401	392	3	0.0667(5)	6.207(15)
O_2	$32^3 \times 64$	6.42	405	240	4	0.0500(4)	11.228(31)
O_3	$48^3 \times 96$	6.59	458	160	5	0.0402(3)	17.630(53)
O_4	$64^3 \times 128$	6.71	74	160	10	0.0345(4)	24.279(227)
P_1	$24^3 \times 48$	6.21	401	280	3	0.0667(5)	6.197(15)
P_2	$32^3 \times 64$	6.42	401	176	4	0.0500(4)	11.270(38)
P_3	$48^3 \times 96$	6.59	191	64	5	0.0402(3)	18.048(152)

TABLE I. Simulation parameters for the HMC algorithm. O and P refer to ensembles with open and periodic boundary condition in the temporal direction. N_{cnfg} is the total number of measurements while ‘Gap’ denotes the interval between two successive measurements in units of τ , the molecular dynamics trajectory length and t_0/a^2 is the dimensionless reference Wilson flow time.

in this case, errors are somewhat under-estimated. Lattice spacings for different ensembles are determined using the results from Refs. [33, 34].

With periodic boundary condition, in order to increase statistics, source averaging is usually performed for the measurement of TCDC. However, with open boundary condition, one cannot do so as translational invariance is lost in the temporal direction. In order to avoid boundary effects in this case, while calculating TCDC, the source is kept at the mid-point of the temporal extent and an averaging over the spatial volume is done. For a meaningful comparison between the results for open and periodic lattices, we adapt the same source averaging procedure for the latter case also.

III. NUMERICAL RESULTS

A. Topological charge density correlator

The Topological Charge Density Correlator (TCDC) is given by

$$C(r) = \langle q(x)q(y) \rangle, \quad r = |x - y| \quad (1)$$

where $q(x)$ is the topological charge density. In order to extract the continuum properties of TCDC from lattice simulations, smoothing of gauge fields is necessary if one uses the field theoretic definition of topological charge density. Unlike observables such as hadron masses and topological susceptibilities, properties of TCDC depend on the energy scale at which one is probing the system. Thus when we compare TCDC at different lattice spacings using smeared gauge configurations, one has to ensure that the smearing is performed at a given energy scale.

In conventional smearing techniques like HYP smearing, a fixed smearing level does not correspond to a common energy scale to compare data generated at different lattice spacings. In Fig. 1, TCDCs at various lattice scales are compared at the same smearing level 3 (HYP). From the exhibited behavior one may infer large scaling violations but one should keep in mind that a fixed HYP smearing level at different lattice spacings does not correspond to a common energy scale. This is to be contrasted with Wilson flow case, which facilitates the use of a common energy scale, shown in the Fig. 2.

Unlike conventional smearing techniques, Wilson flow provides an energy scale ($\frac{1}{\sqrt{8t}}$) at which observables can be probed. In order to check possible scaling violation in TCDC, one has to choose a particular Wilson flow time for all the lattice spacings investigated. In Fig. 2, we plot TCDC for ensembles O_1 , O_2 , O_3 and O_4 at the Wilson flow time $\sqrt{8t} = 0.14$ fm (the rationale for choosing the scale to be 0.14 fm will be explained later). Except the data corresponding to the largest lattice spacing, the data show universal behavior within our statistical uncertainties.

Recently a comparison of Wilson flow with cooling has been performed [35] where a relation between Wilson flow time and the number of cooling steps has been established. We have investigated whether one can phenomenologically establish a relation between Wilson flow time and HYP smearing level. In the case of TCDC, we found that it is not possible to establish such a relation even at a fixed lattice spacing, valid for all r . Some approximate relation, of course can be found, which however, will vary with lattice spacing. This issue needs further investigation in the future.

It is expected that the radius of the positive core of $C(r)$ extracted from lattice data shrinks to zero in the continuum limit. In order to investigate this phenomena first we need to demonstrate the scaling behavior of $C(r)$ extracted at

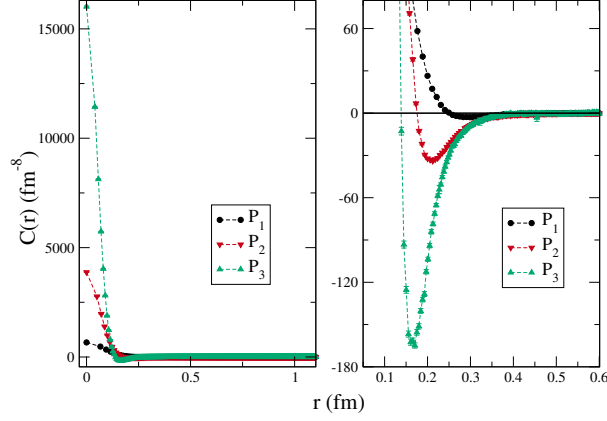


FIG. 1. $C(r)$ versus r at 3 HYP smearing steps for ensembles P_1 , P_2 and P_3 .

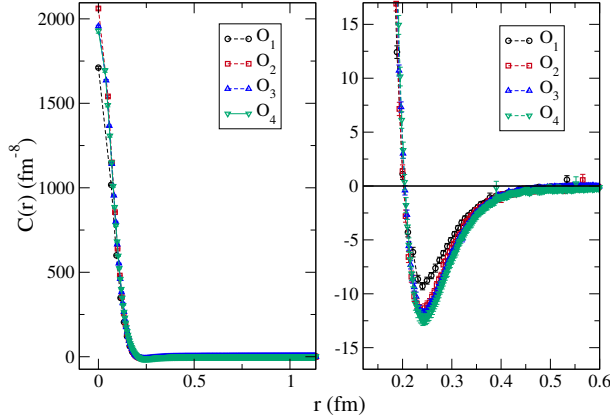


FIG. 2. $C(r)$ versus r at Wilson flow time $\sqrt{8t} = 0.14$ fm for ensembles O_1 , O_2 , O_3 and O_4 .

different lattice spacings, probed at a given Wilson flow time. Then we need to study the behavior of $C(r)$ as Wilson flow time goes to zero to extract the continuum behavior. In Fig. 3, we plot $C(r)$ versus r at various values of Wilson flow time $\sqrt{8t}$ at $\beta = 6.42$ and $\beta = 6.59$ for ensembles P_2 (filled triangle) and P_3 (filled square) respectively. At each Wilson flow time probed the data corresponding to two different lattice scale approximately give the same radius of positive core of $C(r)$. The agreement is approximate partly because the matching of $\sqrt{8t}$ for two different lattice spacings is approximate. We also observe that the radius of the positive core of $C(r)$ decreases as Wilson flow time decreases as expected.

After investigating the scaling behavior, next, we explore the properties of $C(r)$ in detail. Without loss of generality we look at the data at a particular lattice spacing corresponding to $\beta = 6.42$. In Fig. 4, we plot the behavior of $C(r)$ versus r at various Wilson flow times $\sqrt{8t}$ at $\beta = 6.42$ and lattice volume $32^3 \times 64$ for ensemble P_2 . Topological charge density which is constructed from the clover definition of the field strength tensor further gets extended with Wilson flow time. As already shown in Fig. 3, the size of the positive core decreases with decreasing Wilson flow time as presented in Fig. 4. Note that, further, the heights of the positive and negative peaks increase with decreasing flow time. Since with increasing flow time, the effective size of the charge density increases, two charge densities eventually overlap completely resulting in the disappearance of the negative region of $C(r)$.

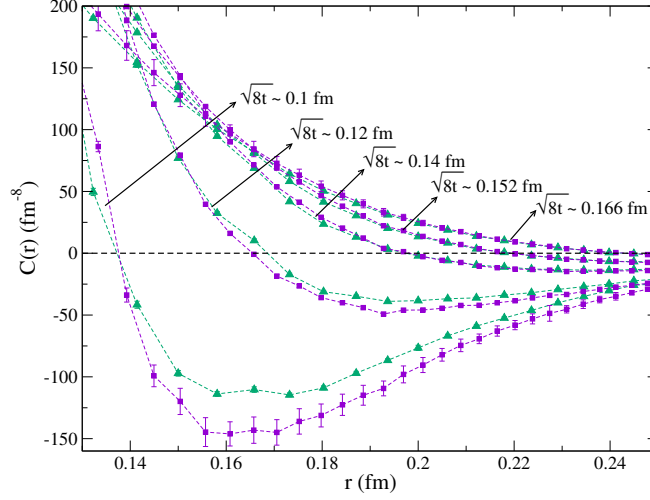


FIG. 3. Plot of $C(r)$ versus r at various values of Wilson flow time $\sqrt{8}t$ at $\beta = 6.42$ and $\beta = 6.59$ for ensembles P_2 (filled triangle) and P_3 (filled square) respectively.

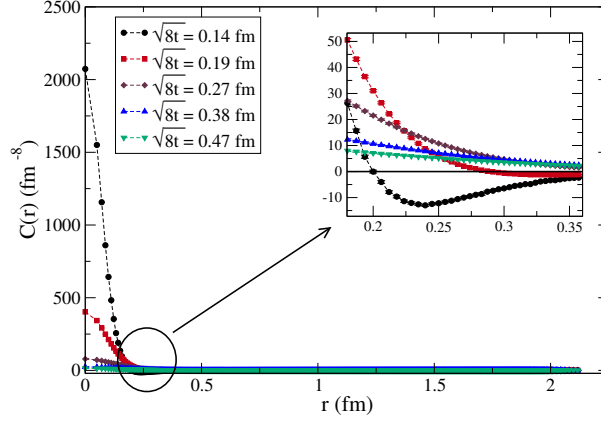


FIG. 4. Plot of topological charge density correlator $C(r)$ versus r at various value of Wilson flow time $\sqrt{8}t$ at $\beta = 6.42$ and lattice volume $32^3 \times 64$ for ensemble P_2 .

In Fig. 5, we compare TCDC for the ensembles P_2 and O_2 . We note that there is no noticeable difference between the two TCDC at a given Wilson flow time. Similar trend has been observed for other lattice spacings as well.

In the Fig. 6, we plot the the radius of the positive core (r_c) versus the Wilson flow time $\sqrt{8}t$ for the ensembles P_2 (filled symbols) and O_2 (open symbols). As noted before, for larger values of Wilson flow time TCDC is always positive. As expected, the radius of the positive core r_c diminishes as Wilson flow time decreases signalling the behavior expected in the continuum.

In the Fig. 7, we plot the unsmeared TCDC for the ensembles O_1 , O_2 , O_3 and O_4 . In this case, presence of severe lattice artifacts prevents one from extracting any physical observable. For example one can not extract the topological susceptibility from such data. Nevertheless we find that the correlator exhibits the negativity as expected for the correlator of pseudo scalar operator. Further we find that the radius of the positive core shrinks with lattice spacing as per expectation.

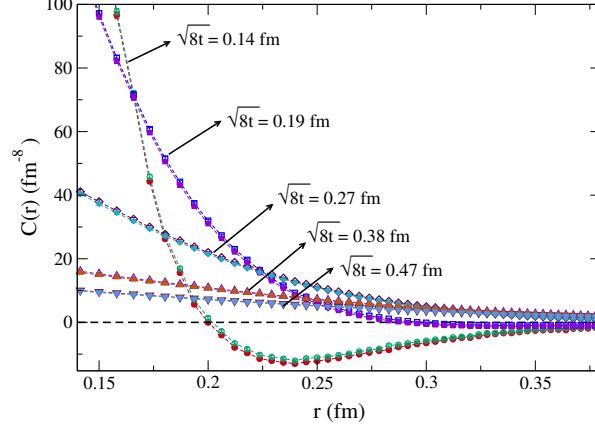


FIG. 5. Comparison of $C(r)$ versus r at various value of Wilson flow time $\sqrt{8}t$ at $\beta = 6.42$ and lattice volume $32^3 \times 64$ for ensembles P_2 (filled symbols) and O_2 (open symbols).

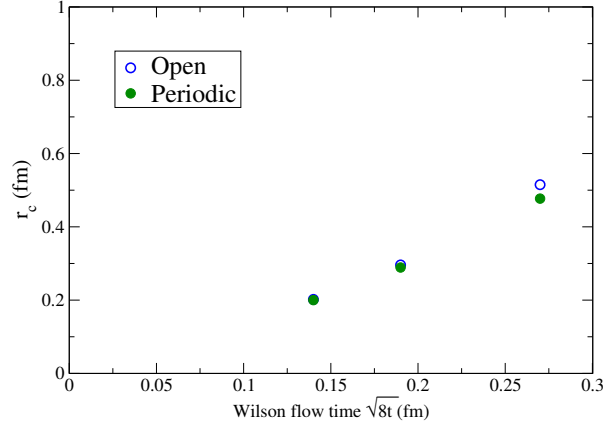


FIG. 6. Plot of r_c versus the Wilson flow time $\sqrt{8}t$ for the ensembles P_2 (filled symbols) and O_2 (open symbols).

B. Extraction of pseudoscalar glueball mass from TCDC

Encouraged by the universal behavior exhibited by the TCDC for different lattice spacings at a common Wilson flow time, we proceed to extract the lowest pseudoscalar glueball mass from the tail region of the TCDC. Due to large vacuum fluctuations present in the correlators of gluonic observables, the extraction of glueball masses is much more difficult compared to hadron masses. In QCD, Ref. [36] proposed the extraction of pseudoscalar flavor singlet meson mass from topological charge density correlator to avoid *the complexity of separating connected and disconnected quark diagrams with potentially large statistical fluctuations*. In Yang-Mills theory, the extraction of pseudoscalar glueball mass from TCDC avoids the same complexity. Since TCDC has severe singularities and lattice artifacts, smoothing of gauge fields is mandatory. Undersmearing of gauge fields leads to persisting lattice artifacts while oversmearing may wipe out even the negativity character of the correlator. Thus there is an optimal range of smearing for which one can reliably extract useful information from the lattice data. Further, the pseudoscalar glueball mass is expected to be much higher than scalar glueball mass. Thus one needs larger statistics and lower lattice spacings for the extraction of pseudoscalar glueball mass. Apart from the cost associated with generating configurations, the cost of measuring all to all radial correlator also increases rapidly as one goes to smaller lattice spacings keeping the physical volume

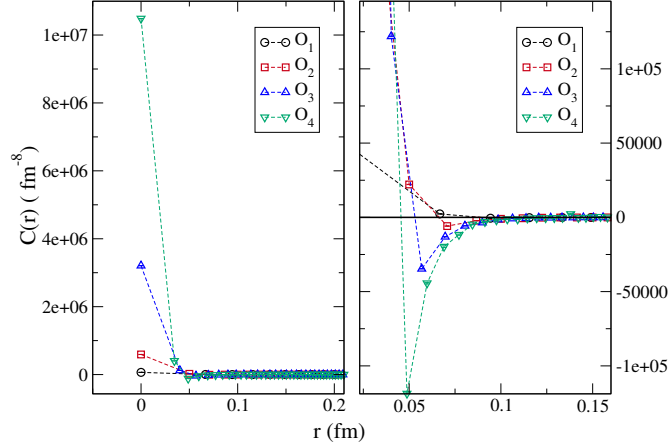


FIG. 7. Plot of $C(r)$ versus r for ensembles O_1 , O_2 , O_3 and O_4 without smoothing of gauge fields.

constant.

In the past MILC collaboration [9] checked the consistency of their quenched correlator data using pseudoscalar glueball mass extracted in Ref. [37] which used anisotropic lattices, as an input without actually fitting the data. In this case, a particular level of HYP smearing is used to smooth the gauge configurations at different lattice spacings.

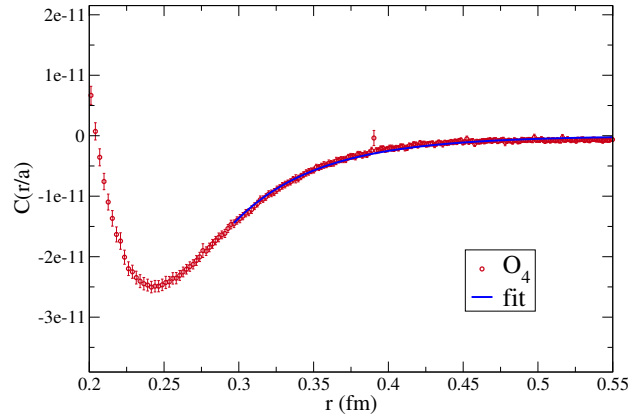


FIG. 8. $C(r/a)$ versus r for the ensemble O_4 at Wilson flow time $\sqrt{8t} = 0.14$ fm. Also shown is the the fit used to extract the pseudoscalar glueball mass.

A formula for TCDC is derived in Appendix B of Ref. [38] for QCD. This is in the context of a leading term in an effective Lagrangian approach originally proposed by Rosenzweig, Schechter and Trahern [39] and by Di Vecchia and Veneziano [40]. This approach has been further developed, being motivated by instanton inspired considerations. In the analysis of the lattice data, the following functional form [38] of the correlator in the negative region is used to extract the pseudoscalar glueball mass:

$$\langle \phi(x)\phi(y) \rangle = \frac{m}{4\pi^2 r} K_1(mr) \quad (2)$$

where $K_1(z)$ is a modified Bessel function whose asymptotic form is given by

$$K_1(z) \underset{\text{large } z}{\sim} e^{-z} \sqrt{\frac{\pi}{2z}} \left[1 + \frac{3}{8z} \right]. \quad (3)$$

Lattice	r_{\min} (fm)	am	m (MeV)
O_1	0.31	0.887(39)	2624(114)
P_1	0.30	0.831(36)	2459(108)
O_2	0.29	0.648(18)	2590(78)
P_2	0.33	0.648(25)	2560(100)
O_3	0.28	0.535(29)	2625(140)
P_3	0.27	0.524(17)	2573(81)
O_4	0.31	0.445(11)	2545(63)

TABLE II. Pseudoscalar glueball mass in lattice and physical units. The starting point of the fit range is denoted by r_{\min} .

In Fig. 8, the TCDC $C(r/a)$ is plotted versus r for the ensemble O_4 at Wilson flow time $\sqrt{8t} = 0.14$ fm. Also shown is the fit in large r region with the formula given in Eq. (3) to extract the pseudoscalar glueball mass. In the fitting procedure the amplitude and the mass are treated as free parameters. We studied the stability of the fit results (mass and amplitude) with fitting range by varying both the initial and the final values of r in the tail region of TCDC.

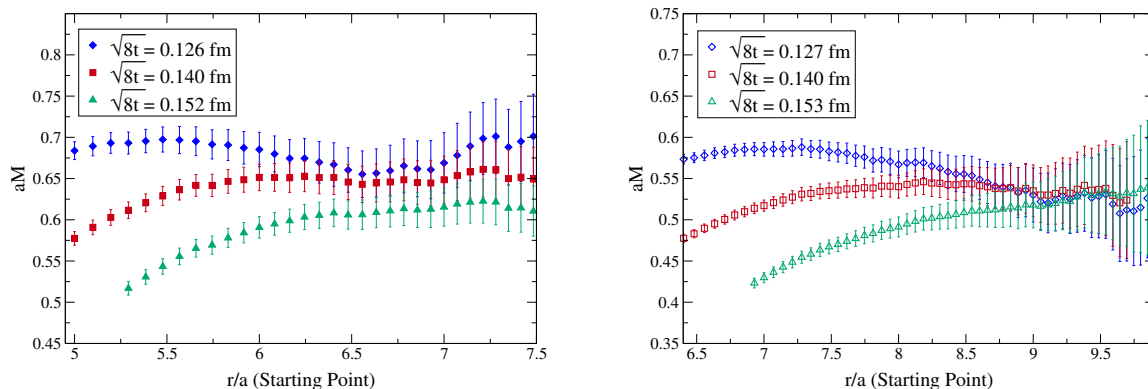


FIG. 9. Sensitivity, to starting point of fit range for fixed end point, of pseudoscalar glueball mass extracted using the asymptotic formula for ensemble P_2 (left) and ensemble O_3 (right).

We have studied the behavior of the extracted pseudoscalar glueball mass under different Wilson flow times. In Fig. 9, we show the sensitivity of the extracted mass to starting point of fit range for a chosen end point, for the ensembles P_2 (left) and O_3 (right). The end point is then varied over a very wide range and examined the stability of the fit for a given starting point. We found that the extracted mass is independent of the end point once the error bar of the tail of the correlator touches the value zero. The extracted mass is apparently stable at and around the scale 0.14 fm as exhibited in the overlap of plateau regions of data for three different Wilson flow times. The overlap between the plateau regions is better for the ensemble O_3 compared to the ensemble P_2 . This behavior is expected as one approaches the continuum. The extracted mass values for different ensembles are given in table II. Since the extracted mass is independent of the end point, we do not quote a specific value in the table. As ensemble sizes for P_3 and O_4 are comparatively small, results for these two ensembles may have some bias leading to possible underestimation of errors as well.

In order to extract the pseudoscalar glueball mass in the continuum, in Fig. 10 we plot the mass in MeV versus a^2 in fm^2 for both the boundary conditions for all the lattice spacings explored in this work. As expected from the universal scaling behavior exhibited by $C(r)$ in the asymptotic region (see Fig. 2) within the statistical error, the data for mass does not show any deviation from scaling. Hence we fit a constant to the data as shown in the figure and thus extract the continuum value of the pseudoscalar glueball mass as 2563 (34) MeV. This value compares very well with the value 2560 (35) MeV quoted in Ref. [37], which is extracted from the decay of the temporal pseudoscalar correlator on an anisotropic lattice.

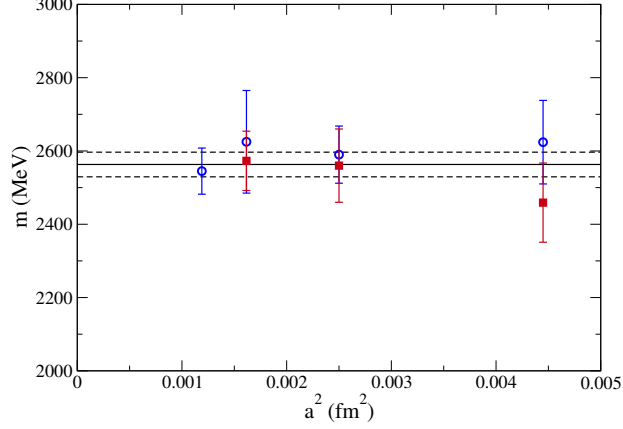


FIG. 10. Plot of lowest pseudoscalar glueball mass versus a^2 for both open (open symbols) and periodic (filled symbols) boundary conditions at Wilson flow time $\sqrt{8}t = 0.14$ fm. Also shown is the fit to the data.

C. Localization properties of topological charge density

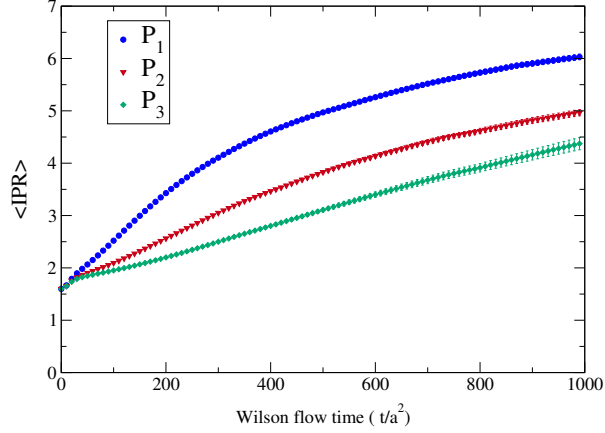


FIG. 11. Plot of configuration average of Inverse Participation Ratio ($\langle \text{IPR} \rangle$) versus Wilson flow time (t/a^2) for the ensembles P_1 , P_2 and P_3 .

It is interesting to study the localization property of the topological charge density $q(x)$ and its behavior under Wilson flow. Since Wilson flow time provides an energy scale to probe the system, it becomes possible to extract the continuum behavior by studying the small Wilson flow time behavior of the observables.

As a measure of the localization property of $q(x)$, one can use the Inverse Participation Ratio (IPR) defined as [31, 32]

$$\text{IPR} = V \frac{\sum_x |q(x)|^4}{(\sum_x |q(x)|^2)^2} \quad (4)$$

where V is the four dimensional lattice volume. If $q(x)$ is completely local, for example $q(x) = \delta(x_0)$, $\text{IPR} = V$ and if $q(x)$ is completely delocalized, $q(x) = c$, a constant then $\text{IPR} = 1$. If $q(x)$ is localized on a fraction of sites f then $\text{IPR} = \frac{1}{f}$ [32]. Thus measurement of IPR provides information about the localization properties of $q(x)$. For an

excellent discussion on IPR [41] which was originally introduced in the context of condensed matter systems, see Ref. [42].

To investigate the effect of Wilson flow on the localization property of topological charge density, we plot the configuration average of IPR versus Wilson flow time (t/a^2) in Fig. 11 for the ensembles P_1 , P_2 and P_3 . We note that $\langle IPR \rangle$ monotonously decreases with decreasing flow time (t/a^2) indicating reduced localization of $q(x)$. Also, *throughout* the range of t/a^2 , $\langle IPR \rangle$ appears to decrease with decreasing lattice spacing.

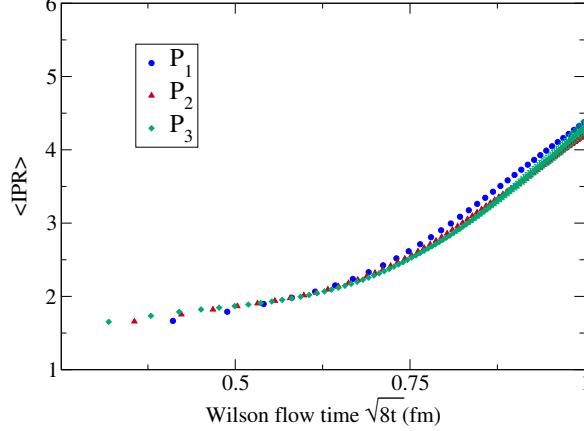


FIG. 12. $\langle IPR \rangle$ versus $\sqrt{8t}$ for ensembles P_1 , P_2 and P_3 .

Since Wilson flow provides a scale (independent of the lattice spacing) to probe the observables, it is more interesting to study the variation of $\langle IPR \rangle$ with respect to $\sqrt{8t}$ for ensembles at different lattice spacings. In Fig. 12 we plot $\langle IPR \rangle$ versus t/r_0^2 for ensembles P_1 , P_2 and P_3 . We find that, remarkably, unlike the behavior shown in figure 11, the average IPR's for different ensembles are now very close to each other and the average IPR's for the ensembles corresponding to the smaller two lattice spacings agree with each other within our statistical accuracy. The data for ensembles corresponding to the largest lattice spacing ($\beta = 6.21$) exhibits some mild scaling violation as already noted in the case of TCDC in Fig. 2. We note that, interestingly, IPR is small for small Wilson flow time and monotonously increases as Wilson flow time increases. This indicates that when probed at short distances $q(x)$ is very much delocalized. On the other hand when probed at long distances $q(x)$ appears more localized.

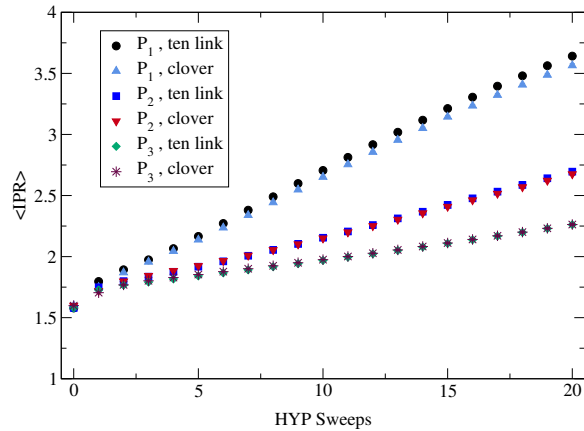


FIG. 13. Plot of $\langle IPR \rangle$ versus HYP sweeps using two definitions of the topological charge density (clover and ten link) for ensembles P_1 , P_2 and P_3 .

Among the available algebraic definitions for $q(x)$, one is based on the clover expression for the field strength $F_{\mu\nu}$ which is the simplest. Another is the more sophisticated ten-link definition developed for $SU(2)$ by DeGrand,

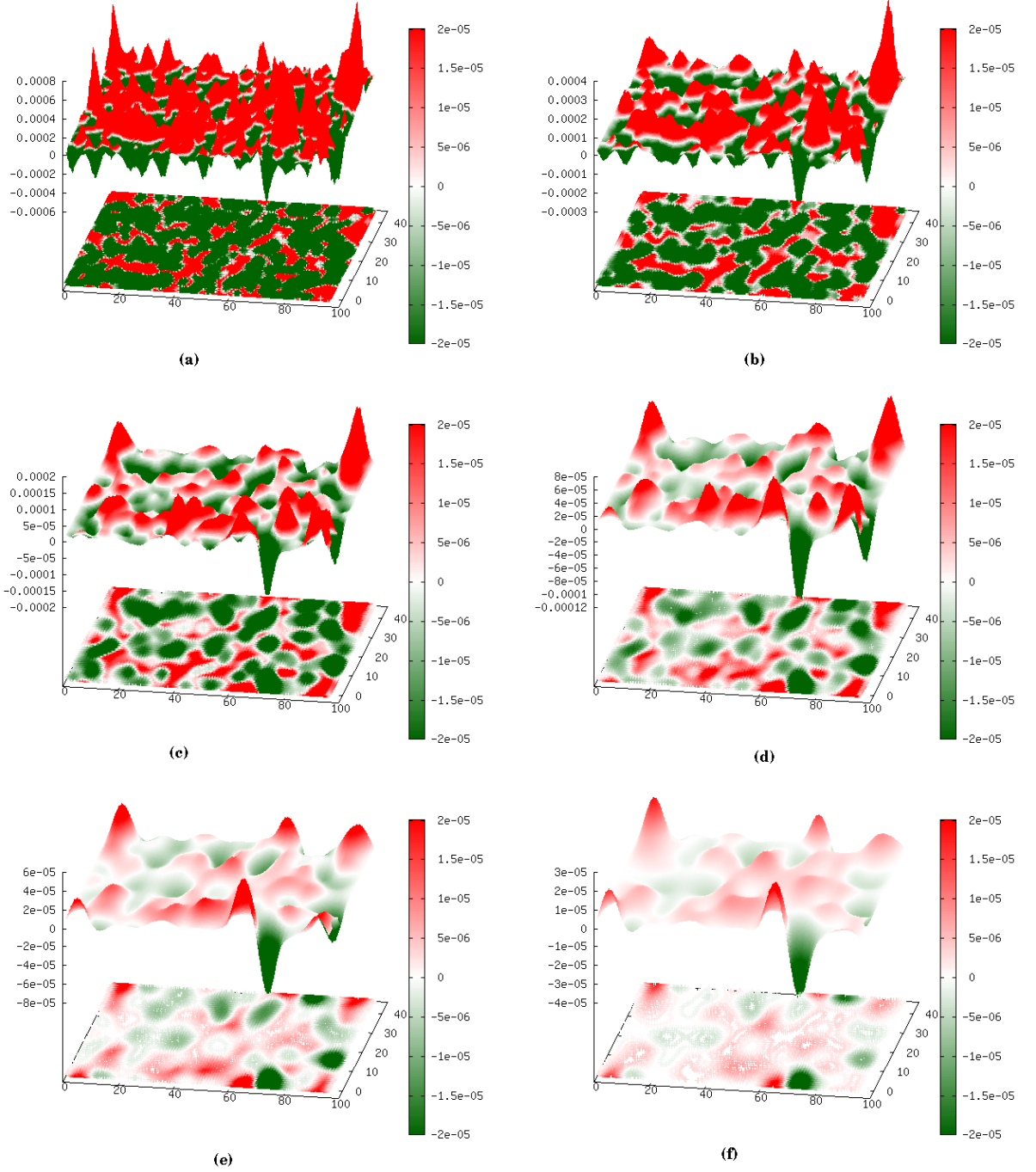


FIG. 14. The behavior of the topological charge density distribution $q(x)$ under Wilson flow, as a function of x_0 and x_1 at $x_2 = x_3 = 24$ for a typical configuration belonging to the ensemble O_3 . The plots (a) to (f) correspond to the flow times $\sqrt{8t} = 0.14, 0.19, 0.25, 0.3, 0.38$ and 0.47 fm respectively.

Hasenfratz and Kovacs [43], modified for $SU(3)$ by Hasenfratz and Neiter [44]. Also there are studies employing tree level improvement over the clover definition of $q(x)$ (as well as the action for cooling process) in case of $SU(2)$ gauge theory [45]. In Fig. 13, we plot $\langle \text{IPR} \rangle$ versus HYP sweeps using two definition of topological charge density (clover and ten link) for ensembles P_1, P_2 and P_3 . It is expected that different lattice discretizations of the topological charge density yield the same physical observable as one approaches the continuum limit. We note that the $\langle \text{IPR} \rangle$ for the two definitions of topological charge density move closer to each other with decreasing lattice spacing, as expected.

We also note that $\langle \text{IPR} \rangle$ decreases with decreasing lattice spacing at a given flow time. The behavior we have observed appears compatible with that exhibited by the data of MILC collaboration [32] at their three smaller lattice

spacings. Note that the largest lattice spacing explored in our work is smaller than the smallest lattice spacing studied in Ref. [32] which, however, has employed an improved lattice action.

In order to gain a better understanding of the behavior of both the charge density correlator $C(r)$ and the inverse participation ratio (IPR) we plot, in Fig. 14, the behavior of the topological charge density distribution $q(x)$ under Wilson flow, as a function of x_0 and x_1 at $x_2 = x_3 = 24$ for a typical configuration belonging to the ensemble O_3 . The plots (a) to (f) correspond to the flow times $\sqrt{8}t = 0.14, 0.19, 0.25, 0.3, 0.38$ and 0.47 fm respectively. In the continuum, it is expected that TCDC possess a positive core and a negative peak adjacent to each other and close to origin. This continuum behavior can be probed through the small values of Wilson flow time. At relatively small values of the Wilson flow time, it is seen that $q(x)$ possesses regions of both positive and negative charge densities of relatively large magnitudes lying next to each other. This provides a qualitative explanation [46] of the positive core and the adjoining negative peak observed in $C(r)$. As the Wilson flow time decreases, the proximity of the regions of positive and negative charge densities of large magnitudes increases, and the charge density appears to be more delocalized. This results in increased participation for $q(x)$ which in turn, explains the decrease of IPR with decreasing Wilson flow time as discussed previously.

In the past, there have been studies (see, for example, Refs. [3, 6, 32] of the fractal dimension of the topological charge density, which have used the Ginsparg-Wilson definition of the topological charge density and improved actions, but at considerably large lattice spacings compared to present standards. Our study of the IPR, on the other hand, has utilized the Wilson action at much smaller lattice spacings and the field strength definition of the topological charge density together with the Wilson flow to smooth the gauge configurations. It will be very interesting to extend the previous studies of the fractal dimension to much smaller lattice spacings together with the use of Wilson flow to study the fractal dimension as a function of the flow time, to avoid any possible contamination of lattice artifacts so that one can reach definite conclusions. Our current study nevertheless seems to support the notion that *the structure of the vacuum of Yang-Mills theory depends on the scale at which it is probed* [31].

IV. CONCLUSIONS

In SU(3) Lattice Yang-Mills theory, we have investigated TCDC and IPR of topological charge density ($q(x)$) for a range of relatively small lattice spacings with the view of studying the continuum properties. As expected we have not found any noticeable difference between periodic and the recently proposed open boundary conditions. However, open boundary condition has enabled us to compute observables at a smaller lattice spacing because of the absence of the *trapping problem*. Recently proposed Wilson flow, in contrast to the smearing techniques proposed previously, provides a common energy scale to probe the system simulated for variety of lattice spacings. In contrast to a fixed HYP smearing level, by choosing a particular Wilson flow time t for all the lattice spacings investigated, we find that, except the data corresponding to the largest lattice spacing, the TCDC data show universal behavior within our statistical uncertainties. The continuum properties of TCDC are inferred by the studying the small flow time behavior. The pseudoscalar glueball mass obtained from the tail region of TCDC does not exhibit any noticeable scaling violation and the extracted value in the continuum, 2563 (34) MeV agrees well with the value extracted previously in the literature with anisotropic lattices. We found that the configuration average of the inverse participation ratio for topological charge density, calculated at a given level of smearing (for the Wilson flow it is t/a^2) decreases with the lattice spacing. However when plotted versus common scale $\sqrt{8}t$, it seems to be independent of lattice spacing. A detailed study of $q(x)$ under Wilson flow time revealed that as Wilson flow time decreases, the proximity of the regions of positive and negative charge densities of large magnitudes increases, and the charge density appears to be more delocalized resulting in the observed decrease of IPR with decreasing Wilson flow time.

ACKNOWLEDGMENTS

To carry out all the numerical calculations reported in this work, Cray XT5 and Cray XE6 systems supported by the 11th-12th Five Year Plan Projects of the Theory Division, SINP under the Department of Atomic Energy, Govt. of India, are used. We thank Richard Chang for the prompt maintenance of the systems and the help in data management. For some useful discussions, we also thank Pushan Majumdar and Santanu Mondal. We are indebted to Philippe de Forcrand for helpful comments on the earlier version of this manuscript. This work was in part based

on the publicly available lattice gauge theory code `openQCD` [47] and that of MILC collaboration [48] .

-
- [1] E. Seiler and I. O. Stamatescu, *Some remarks on the Witten-Veneziano formula for the eta-prime mass*, MPI-PAE/PTh 10/87, unpublished.
 - [2] E. Seiler, *Some more remarks on the Witten-Veneziano formula for the eta-prime mass*, Phys. Lett. B **525**, 355 (2002) [hep-th/0111125].
 - [3] I. Horvath, S. J. Dong, T. Draper, F. X. Lee, K. F. Liu, N. Mathur, H. B. Thacker and J. B. Zhang, *Low dimensional long range topological charge structure in the QCD vacuum*, Phys. Rev. D **68**, 114505 (2003) [hep-lat/0302009].
 - [4] A. Hasenfratz, *Spatial correlation of the topological charge in pure SU(3) gauge theory and in QCD*, Phys. Lett. B **476**, 188 (2000) [hep-lat/9912053].
 - [5] I. Horvath, A. Alexandru, J. B. Zhang, Y. Chen, S. J. Dong, T. Draper, K. F. Liu, N. Mathur, S. Tamhankar and H. B. Thacker, *The negativity of the overlap-based topological charge density correlator in pure-gluon QCD and the non-integrable nature of its contact part*, Phys. Lett. B **617**, 49 (2005) [hep-lat/0504005].
 - [6] E.-M. Ilgenfritz, K. Koller, Y. Koma, G. Schierholz, T. Streuer and V. Weinberg, *Exploring the structure of the quenched QCD vacuum with overlap fermions*, Phys. Rev. D **76**, 034506 (2007) [arXiv:0705.0018 [hep-lat]].
 - [7] E.-M. Ilgenfritz, D. Leinweber, P. Moran, K. Koller, G. Schierholz and V. Weinberg, *Vacuum structure revealed by over-improved stout-link smearing compared with the overlap analysis for quenched QCD*, Phys. Rev. D **77**, 074502 (2008) [Erratum-ibid. D **77**, 099902 (2008)] [arXiv:0801.1725 [hep-lat]].
 - [8] P. J. Moran and D. B. Leinweber, *Impact of Dynamical Fermions on QCD Vacuum Structure*, Phys. Rev. D **78**, 054506 (2008) [arXiv:0801.2016 [hep-lat]].
 - [9] A. Bazavov *et al.* [MILC Collaboration], *Topological susceptibility with the asqtad action*, Phys. Rev. D **81**, 114501 (2010) [arXiv:1003.5695 [hep-lat]].
 - [10] F. Bruckmann, F. Gruber, N. Cundy, A. Schafer and T. Lippert, *Topology of dynamical lattice configurations including results from dynamical overlap fermions*, Phys. Lett. B **707**, 278 (2012) [arXiv:1107.0897 [hep-lat]].
 - [11] A. Chowdhury, A. K. De, A. Harindranath, J. Maiti and S. Mondal, *Topological charge density correlator in lattice QCD with two flavours of unimproved Wilson fermions*, JHEP **11**, 029 (2012) [arXiv:1208.4235 [hep-lat]].
 - [12] M. Bruno, S. Schaefer and R. Sommer, *Topological susceptibility and the sampling of field space in $N_f = 2$ lattice QCD simulations*, JHEP **08**, 150 (2014) [arXiv:1406.5363 [hep-lat]].
 - [13] H. Fukaya *et al.* [JLQCD Collaboration], *Topology density correlator on dynamical domain-wall ensembles with nearly frozen topological charge*, arXiv:1411.1473 [hep-lat].
 - [14] E. Witten, *Current Algebra theorems for the U(1) Goldstone boson*, Nucl. Phys. B **156**, 269 (1979).
 - [15] G. Veneziano, *U(1) without instantons*, Nucl. Phys. B **159**, 213 (1979).
 - [16] S. Dürr, Z. Fodor, C. Hoelbling and T. Kurth, *Precision study of the SU(3) topological susceptibility in the continuum*, JHEP **0704**, 055 (2007) [hep-lat/0612021].
 - [17] L. Del Debbio, L. Giusti and C. Pica, *Topological susceptibility in the SU(3) gauge theory*, Phys. Rev. Lett. **94**, 032003 (2005) [hep-th/0407052].
 - [18] M. Lüscher, *Topological effects in QCD and the problem of short distance singularities*, Phys. Lett. B **593**, 296 (2004) [hep-th/0404034].
 - [19] L. Giusti and M. Lüscher, *Chiral symmetry breaking and the Banks-Casher relation in lattice QCD with Wilson quarks*, JHEP **0903**, 013 (2009) [arXiv:0812.3638 [hep-lat]].
 - [20] M. Lüscher and F. Palombi, *Universality of the topological susceptibility in the SU(3) gauge theory*, JHEP **1009**, 110 (2010) [arXiv:1008.0732 [hep-lat]].
 - [21] M. Lüscher, *Topology, the Wilson flow and the HMC algorithm*, PoS LATTICE **2010**, 015 (2010) [arXiv:1009.5877 [hep-lat]].
 - [22] M. Lüscher and S. Schaefer, *Lattice QCD without topology barriers*, JHEP **1107**, 036 (2011) [arXiv:1105.4749 [hep-lat]].
 - [23] M. Lüscher and S. Schaefer, *Lattice QCD with open boundary conditions and twisted-mass reweighting*, Comput. Phys. Commun. **184**, 519 (2013) [arXiv:1206.2809 [hep-lat]].
 - [24] M. Grady, *Connecting phase transitions between the 3-d O(4) Heisenberg model and 4-d SU(2) lattice gauge theory*, arXiv:1104.3331 [hep-lat].
 - [25] A. Hasenfratz and F. Knechtli, *Flavor symmetry and the static potential with hypercubic blocking*, Phys. Rev. D **64**, 034504 (2001) [hep-lat/0103029].
 - [26] M. Lüscher, *Trivializing maps, the Wilson flow and the HMC algorithm*, Commun. Math. Phys. **293**, 899 (2010) [arXiv:0907.5491 [hep-lat]].
 - [27] M. Lüscher, *Properties and uses of the Wilson flow in lattice QCD*, JHEP **1008**, 071 (2010) [arXiv:1006.4518 [hep-lat]].
 - [28] M. Lüscher and P. Weisz, *Perturbative analysis of the gradient flow in non-abelian gauge theories*, JHEP **1102**, 051 (2011) [arXiv:1101.0963 [hep-th]].
 - [29] A. Chowdhury, A. Harindranath, J. Maiti and P. Majumdar, JHEP **02**, 045 (2014) *Topological susceptibility in lattice Yang-Mills theory with open boundary condition*, [arXiv:1311.6599 [hep-lat]].
 - [30] A. Chowdhury, A. Harindranath and J. Maiti, *Open boundary condition, Wilson Flow and the scalar Glueball mass*, JHEP **1406**, 067 (2014) [arXiv:1402.7138 [hep-lat]].

- [31] For a review, see, P. de Forcrand, *Localization properties of fermions and bosons*, AIP Conf. Proc. **892**, 29 (2007) [hep-lat/0611034].
- [32] C. Aubin *et al.* [MILC Collaboration], *The scaling dimension of low lying Dirac eigenmodes and of the topological charge density*, Nucl. Phys. Proc. Suppl. **140**, 626 (2005) [hep-lat/0410024].
- [33] M. Guagnelli, R. Sommer and H. Wittig [ALPHA Collaboration], *Precision computation of a low-energy reference scale in quenched lattice QCD*, Nucl. Phys. B **535**, 389 (1998) [hep-lat/9806005].
- [34] S. Necco and R. Sommer, *The $N_f = 0$ heavy quark potential from short to intermediate distances*, Nucl. Phys. B **622**, 328 (2002) [hep-lat/0108008].
- [35] C. Bonati and M. D’Elia, *Comparison of the gradient flow with cooling in $SU(3)$ pure gauge theory*, Phys. Rev. D **89**, 105005 (2014) [arXiv:1401.2441 [hep-lat]].
- [36] M. Creutz, *Anomalies, gauge field topology, and the lattice*, Annals Phys. **326**, 911 (2011) [arXiv:1007.5502 [hep-lat]].
- [37] Y. Chen *et al.*, *Glueball spectrum and matrix elements on anisotropic lattices*, Phys. Rev. D **73**, 014516 (2006) [hep-lat/0510074].
- [38] E. V. Shuryak and J. J. M. Verbaarschot, *Screening of the topological charge in a correlated instanton vacuum*, Phys. Rev. D **52**, 295 (1995).
- [39] C. Rosenzweig, J. Schechter and C. G. Trahern, *Is the effective lagrangian for QCD a sigma model?*, Phys. Rev. D **21**, 3388 (1980).
- [40] P. Di Vecchia and G. Veneziano, *Chiral dynamics in the large N limit*, Nucl. Phys. B **171**, 253 (1980).
- [41] R.J. Bell and R. Dean, *Atomic vibrations in vitreous silica*, Discuss. Faraday Soc. **50**, 55 (1970).
- [42] F. Wegner, *Inverse participation ratio in $2 + \epsilon$ dimensions*, Z. Physik **B 36**, 209 (1980).
- [43] T. A. DeGrand, A. Hasenfratz, T. G. Kovacs, *Topological structure in the $SU(2)$ vacuum*, Nucl. Phys. **B505**, 417-441 (1997). [arXiv:hep-lat/9705009 [hep-lat]].
- [44] A. Hasenfratz, C. Nieter, *Instanton content of the $SU(3)$ vacuum*, Phys. Lett. **B439**, 366-372 (1998). [hep-lat/9806026].
- [45] P. de Forcrand, M. Garcia Perez and I. O. Stamatescu, *Topology of the $SU(2)$ vacuum: A Lattice study using improved cooling*, Nucl. Phys. B **499**, 409 (1997) [hep-lat/9701012].
- [46] S. Ahmad, J. T. Lenaghan and H. B. Thacker, *Coherent topological charge structure in $CP^{(N-1)}$ models and QCD*, Phys. Rev. D **72**, 114511 (2005) [hep-lat/0509066].
- [47] <http://luscher.web.cern.ch/luscher/openQCD/>.
- [48] <http://physics.indiana.edu/~sg/milc.html>.